Loss of chromogranin A and catestatin affect pancreatic islet homeostasis, endocrine function, and neurotransmitters

(max. 8 words)

Elke M. Muntjewerff[1], Dali Epremidze[1], Mariya Nezhyva[2], Marleen Bootsma[1], Atef Mannaa[3], Hiromi Ikebuchi[1], Anna Nilsson[2,4], Per E. Andrén[2,4], Erik Jansson[2], Sushil K. Mahata[5,6], & Gustaf Christoffersson[1,7*]

[1] Department of Medical Cell Biology, Uppsala University, Sweden
[2] Department of Pharmaceutical Biosciences, Uppsala University, Sweden
[3]INSERM U1192, Laboratoire Protéomique, Réponse Inflammatoire & Spectrométrie de Masse (PRISM), Université de Lille, France.
[4] Spatial Mass Spectrometry Infrastructure Unit, Science for Life Laboratory, Uppsala University, Sweden
[5] VA San Diego Healthcare System, San Diego, CA, USA
[6] Department of Medicine, University of California San Diego, La Jolla, California, USA
[7] Science for Life Laboratory, Uppsala University, Sweden

*** Correspondence:**
Gustaf Christoffersson
ORCID: 0000-0002-9640-9702

Uppsala University
Department of Medical cell Biology
Husargatan 3, 75123 Uppsala
Email: gustaf.christoffersson@scilifelab.uu.se
Tel: +4618-4714325
Fax: +18-471 4325

Journal: Nature communications
Article type: Research paper
Word count: 4101 (including method section)
Figures: 6

Running title: Lack of CgA and CST affects pancreatic islet

Keywords: Neurotransmitters [1], Pancreatic islets[2]; Chromogranin A [3]; Catestatin[4]; Metabolites[5]

Abstract (max. 200)

The pro-hormone chromogranin A (CgA) and its cleavage product, the neuropeptide catestatin (CST) are linked to various cardiovascular and autoimmune diseases (T1D, IBD, RA) as biomarkers for disease severity. In these diseases, CgA and CST seem to affect inflammation, nerve communication, insulin resistance and hypertension. Since we found various CgA

cleavage products leading towards CST in the pancreatic islet, we investigated how CgA and CST may modulate the pancreatic islet microenvironment and function. We show that CgA-KO and CST-KO mice have fewer insulin producing cells per islet and altered physiological islet function. To map the neurotransmitter microenvironment in the pancreatic islet and exocrine tissue we used spatial mass spectrometry that allowed us to identify neurotransmitter levels in and outside of the islets. Using this method, we show that endocrine cell homeostasis and insulin regulating pathways are disturbed in the pancreatic islets upon CgA or CST deletion. Thus, absence of CgA or CST in mice affects the endocrine composition and microenvironment of the pancreatic islet. Our findings contribute to understanding the role of CgA and CST in the pancreas with possible implications for the pathology of both type 1 and type 2 diabetes.

1. Introduction

Chromogranin A (CgA), a 49 kDa pro-hormone, has been extensively studied in the initiation and regulation of dense-core secretory granule biogenesis as well as in the context of various metabolic and inflammatory diseases. Increased circulating CgA levels are linked to various diseases including neuroendocrine tumors [1], hypertension [2,3] *congestive heart failure* [4], *renal failure* [5], *inflammatory bowel disease* [6], *rheumatoid arthritis* [7], *sepsis* [8], *and Alzheimer's disease* [9]. CgA is secreted by endocrine cells such as chromaffin cells in the adrenal medulla, enterochromaffin cells in the gut, beta cells in pancreatic islets, and neurons and immune cells such as neutrophils, monocytes and macrophages [10]. Proteolytic cleavage of the pro-hormone CgA, gives rise to neuropeptides such as catestatin (CST) that exert a wide variety of immune- and neuro-regulatory functions [10]. The 21 amino acid long CST acts as an anti-inflammatory [11–13], anti-diabetic [12] and cardioprotective peptide [14]. Elevated CST blood levels are seen in type 2 diabetes [15], inflammatory bowel disease [6], rheumatoid arthritis [16], COVID-19 infection [17] and various cardiovascular diseases such as acute heart failure, arrhythmia and hypertension [18–24]. Recent studies implicate that higher plasma CST, in combination with low plasma catecholamines, is associated with a worse disease prognosis for heart failure (5-times more death for high plasma CST compared to normal CST) [18–22]. At the same time low plasma CST and high catecholamine levels are associated with type 2 diabetes [15] and other cardiovascular diseases including hypertension [23,24]. In line with this, the supplementation of CST in rodents with hypertension normalized blood pressure [13,25–27], reduces chronic gut inflammation in murine colitis models [28,29] and improved inflammation and insulin sensitivity in mice with diet-induced obesity [12].

Based on the link of CgA and CST to various endocrine diseases and its presence in the pancreatic islets, we aimed to investigate how CgA and its cleavage product CST may influence the pancreatic islet microenvironment and function via studying the effect of CgA and CST deficiency in knock-out mice with respect to 1) pancreatic islet density and shape, 2) endocrine islet composition by staining for alpha (α), beta (β) and delta (δ) cells, and 3) mapping neurotransmitters and metabolites in the pancreatic islet and exocrine tissue using spatial mass spectrometry (MS). For this purpose, we used the pancreas of CgA full knockout mice [25] and mice with selective deletion of the CST-coding region of the *Chga* gene [13]. CgA-KO mice are characterized with hypertension, elevated sympathoneuronal activity and affected endocrine cells in the adrenal gland and pancreas [25,30]. The CST-KO mice are hypertensive, obese and exhibit insulin resistance. Additionally, they display low grade organ inflammation, elevated amounts of norepinephrine and epinephrine in the plasma, lower bacterial gut diversity, and impaired epithelial barrier function [6,12,13].

To our knowledge, this is the first study to comprehensively assess the pancreatic microenvironment, including endocrine cell density and composition, innervation, and spatial MS foridentifying neurotransmitter and metabolite levels. We show that islets lacking CgA and CST display aberrant quotas of alpha- and beta cells, with accompanying differences in blood glucose homeostasis. Various neurotransmitters involved in crucial processes such as hormone regulation were also affected by CgA or CST deletion. Our findings contribute to understanding the role of CgA and CST in the pancreas with possible implications for the pathology of both type 1 and type 2 diabetes.

2 Results

2.1 CgA and CST in the pancreatic islet

To investigate the presence of CST in the pancreatic islets, we stained frozen pancreatic sections of WT, CgA-KO and CST-KO mice. The CST staining appeared in the pancreatic islets in WT mice, whereas CgA or CST knockout pancreata had no CST staining in the pancreatic islets (Fig. 1A). We also observed CST staining outside the pancreatic islets in WT tissue, which could be attributed to immune cells or nerves. At the moment, the exact CgA cleavage products present in the pancreas, including the ones leading to CST are unknown (Fig. 1B). To further confirm the presence of CgA and CST, we compared levels in the adrenal gland medulla, pancreatic islets, and macrophages in WT mice using immunoblotting (Fig. 1C, D). Full-length CgA (75 kDa) was detected in the adrenal gland medulla, but not in the pancreatic islets, which instead exhibited various CgA cleavage products, indicating rapid processing towards for example CST (Fig. 1B). For both macrophages and pancreatic islets, it seems that a product of the size of CST is present since bands appeared similarly to the loaded synthetic CST peptide (Fig. 1C, D). Nevertheless, the presence of multiple CgA cleavage products and CST in the islets implies an active role in maintaining islet homeostasis.

2.2 Islet morphology and endocrine islet composition is altered upon CST or CgA deletion

To get an overview of the pancreas of WT, CgA-KO and CST-KO sections, we made full-section scans of hematoxylin and eosin-stained slides (Fig. 2A). These pictures seemed to show changes in islet morphology, which can indicate aberrations in islet function [31,32]. To investigate pancreatic islet morphology and endocrine cell composition in CgA or CST KO mice in more detail, we stained frozen pancreatic sections of KO mice for insulin, glucagon and somatostatin (Fig. 2B). First, we quantified the islet density and islet area. Although the individual islet areas were unchanged, the islet density was significantly decreased in the CgA-KO pancreas when compared to WT and CST-KO pancreas (Fig. 2C-D), which is in line with previous findings for the CgA-KO mouse islets [30]. Next, the islet shape was assessed, showing decreased islet circularity in CST-KO compared to WT islets (Fig. 2E).

To assess the endocrine islet composition, we identified the alpha, beta and delta cell ratios per islet for WT, CgA-KO and CST-KO mice (Fig. 2F). In line with previous findings [30], the quantification shows that CgA-KO mice display a significant increase in alpha cells and a decrease in beta cells per islet when compared to WT islets. The CST-KO mice only show a decrease in beta cells when compared to the WT islets. In line with these findings, the number of hormone-negative cells in the CST and CgA-KO islets was significantly increased. This means that CgA-KO and CST-KO mice have fewer endocrine cells per islet, which in combination with the decreased islet density in CgA-KO mice may be part of the explanation to altered endocrine function. To investigate how this affects the

physiological function of the islets, we performed an *in vivo* glucose tolerance test (GTT). Here, the deletion of CgA resulted in lower blood glucose levels when compared to the WT glucose levels (Fig. 2G, H). This is surprising, as these mice had a reduction in numbers of beta cells, but could thus mean that they are highly functional and release more than sufficient amounts of insulin or that peripheral tissues are more insulin sensitive as documented previously [33]. A previous study also found that CgA-KO beta cells to contain more insulin granules and to be more responsive to a glucose challenge [30]. In contrast, the lack of CST resulted in increased blood glucose levels when compared to WT. This may instead indicate beta cell dysfunction or insulin resistance as documented previously [12]. Thus, absence of CgA or CST in mice affects the endocrine cell composition and likely also the function of the pancreatic islet in opposite ways.

2.3 Pancreatic sympathetic innervation in mice lacking CgA and CST

There is increasing evidence that the pancreatic islet innervation is disordered in type 1 and type 2 diabetes, which may lead to changes in regulation of islet hormone release and metabolic regulation [34]. To investigate whether the observed changes in endocrine composition and/or function in the CgA-KO and CST-KO mice may be related to the islet innervation, we stained the pancreatic sections for the norepinephrine transporter (NET) to visualize sympathetic neurons (Fig. 3A). Although the nerve network looks more disorganized in the CgA-KO and CST-KO pancreas, the quantification did not reveal major quantitative differences regarding islet innervation between WT, CgA-KO and CST-KO pancreata (Fig. 3B). Comparing innervation in and around the pancreatic islet, the nerve ratio for WT islets was significantly lower when compared to the exocrine nerve network (Fig. 3C). However, this difference between in- and outside the islet was lost for the CgA-KO and CST-KO mice. This might indicate changes in the overall nerve network organization upon CgA or CST deletion. CST acts as a neuropeptide and has been shown to be produced by and have effect on nerves and macrophages, which seems to result in suppression of neuronal and neuroendocrine activity in an inflammation-dependent manner [10]. To investigate its role in the pancreas, we quantified the nerve-macrophage interactions in the pancreatic islets of the CgA and CST-KO mice (Fig. 3D). Although no difference was found in the number of macrophages per islet, we observed a trend for less macrophage-nerve interactions in the islet upon CgA or CST deletion when compared to WT (Fig. 3E, F).

2.4 Neurotransmitter and metabolite levels are changed in CgA-KO and CST-KO pancreas

By spatial MS, we detected 12 pancreatic neurotransmitters and metabolites that met validation criteria (Sup Table 1). Values were extracted for WT, CgA-KO and CST-KO endocrine and exocrine pancreas and the differential expression was visualized in a bar chart (Fig. 4A) These data showed that hypoxanthine, tyrosine, spermidine, histidine, cysteine, spermine levels differ between CST-KO and WT. For most neurotransmitters, the expression seemed to be lowest in the CgA-KO pancreas when compared to WT and CST-KO. Afterwards, we visualized the expression of these analytes in the exocrine and islet part of the pancreas (Fig. 4B). Altogether this, resulted in a comprehensive view of the neurotransmitters in the WT, CgA-KO and CST-KO pancreas.

2.5 Metabolic and neurotransmitter pathways are affected in CgA-KO and CST-KO pancreatic islets.

In addition to the combined analysis, we took a closer look at the individual hits in pancreatic islets and exocrine pancreas to identify which parts of the pathways were affected in the islets and exocrine tissue of CgA-KO and CST-KO pancreas.

To be able to distinguish the neurotransmitter levels between the pancreatic islets and exocrine tissue, we identified the islets on a consecutive section stained with HE. After scanning the pancreatic slice in a microscope, we matched the exported islet regions to the intensity distribution of the serotonin signal and selected the exocrine tissue (serotonin negative) (Fig. 5A). For all three genotypes, serotonin and taurine levels were significantly higher in the pancreatic islets when compared to the exocrine tissue (Fig. 5A-B). Additionally, GABA and histamine levels are higher in the islets when compared to exocrine tissue for WT and CST-KO (Fig. 5D-E). We also noted that CgA-KO showed lower GABA values in islets, and for both GABA and histamine no changes between islet and exocrine tissue where detected. For the CgA-KO islets and exocrine tissue we also observed a decrease in cysteine, compared to WT (Fig. 5F). Cysteine is a highly conserved amino acid involved in regulating catalysis, protein structure, redox sensitivity and metal-ion transport [35]. Decreased cysteine levels might indicate problems within the homocysteine pathway.

Polyamines (spermidine, spermine and thermospine) play an important role in cell growth, proliferation and differentiation. In the pancreas, polyamines seem to modulate beta cell function by affecting proinsulin biosynthesis and insulin secretion [36]. Spermidine is synthesized from putrescine by spermidine synthase. This process takes place in all mice since similar spermidine values were found for WT, CST-KO and CgA-KO pancreas (Fig. 5G). Afterwards, spermidine is normally converted into spermine by spermine synthase. However, this process seems disturbed in the knockout mice since spermine levels are drastically decreased for the CgA-KO and CST-KO islets and exocrine tissue when compared to WT pancreas (Fig. 5G). This suggests that the conversion by spermine synthase is less efficient in the absence of CgA or CST.

Norepinephrine (NE) and dopamine are both catecholamines that can regulate insulin secretion by the pancreatic beta cells [36,37]. Thereby the synthesis and degradation of NE and dopamine are essential for normal function of the pancreas. In the past, increased adrenal and plasma catecholamine levels have been detected in the plasma and adrenal gland of CgA-KO and CST-KO mice [13]. In contrast, our data shows that NE levels in the pancreas seem normal for the CgA-KO and CST-KO mice since we observed high islet NE levels and lower NE exocrine levels for all three genotypes (Fig. 6A). These data suggest that the catecholamine levels in the pancreas are normal, however the catecholamine degradation might still be disturbed.

The creatine pathway seems unaffected since creatine levels appear normal for all three mice (Fig. 6B). Hypoxanthine levels are only significantly increased in the CST-KO mice (Fig. 6C). Here both exocrine tissue and islets show high levels of hypoxanthine, which could indicate pancreatic necrosis[38].

3 Conclusion and discussion

Our study demonstrates that chromogranin A (CgA) and its cleavage product, catestatin (CST), are essential for normal pancreatic islet structure and function. The obtained results show that the absence of CgA or CST leads to altered islet morphology, reduced beta cell

numbers, increased alpha cell numbers, and disrupted neurotransmitter levels, affecting glucose regulation and endocrine homeostasis.

Although the blood circulating levels of CgA and CST are high in autoimmune disease, we found various CgA cleavage products in the pancreas. This indicates that the local balance in the organ does not always resemble the systemic levels. More research on the local pancreatic CgA cleavage products could reveal their balance and their function in this complex neuro-immune interplay in health and disease.

Studies on mouse and human islets showed that the islet size and ratios of alpha to beta cells were related to chronic hyperglycaemia [38]. Similarly to our CgA-KO and CST-KO data, diabetic mice with chronic hyperglycaemia showed a decrease in insulin positive cells and an increase in glucagon positive cells [31]. This indicates that CgA or CST knockout affects pancreatic homeostasis via the endocrine cells. Moreover, previous research showed that CgA-KO islets beta cells have a higher insulin granule content and *in vivo* glucose stimulation resulted in faster insulin release than in WT mice. However, the basal insulin plasma levels in the CgA-KO mouse where lower than for WT [39].

Since the amount of beta cells is decreased in the CgA-KO and CST-KO islets when compared to WT, it might be that the reduction in beta cells is compensated by the production of more insulin granules per cell.

Beta cells contain highest concentrations of polyamines (putrescine, spermidine, and spermine) [40,41] , where they regulate proinsulin biosynthesis and secretion of insulin [42]. The depletion of polyamines in isolated mouse islets has been associated with impaired glucose-stimulated insulin secretion, insulin content, insulin transcription, and DNA replication [43,44]. Polyamine levels were reported to be diminished in aging and obese mice [45], which are resistant to insulin. Therefore, markedly decreased spermine levels in CST-KO pancreas possibly explains insulin resistance in CST-KO mice [12].

Also the observed lower spermine levels in the CgA-KO and CST-KO mice can result in disturbed insulin secretion [36] and less uptake of Ca^{2+} by the beta cells [46]. In obese mice the spermine to spermidine ratio is even similarly disturbed in the pancreatic islets as in our knockout mice [45]. Altogether, more research is necessary to identify the disorganized pathway(s) resulting in the affected islet composition in the CgA-KO and CST-KO mice. With our unique methodology, we were able to spatially investigate the pancreatic microenvironment - a crucial step towards identifying and understanding the disorganized pathways affecting islet composition in knockout mice. However, since our current methodology is insufficient to detect enzyme expression and activity, future research should focus on studying the enzymes regulating catecholamine degradation and spermine pathways to clarify the underlying mechanisms of the pancreatic microenvironment further.

Recent studies have highlighted the crucial connection between the local immune system in the pancreas and the peripheral nervous system in the development of autoimmune diseases [47–49]. Interfering with pancreatic nerve signals through surgery, chemical blockage, or electric stimulation has been shown to preserve sympathetic nerves and prevent the onset of type 1 diabetes (T1D) in mice [47–49] Additionally, depleting macrophages during the onset of autoimmune diabetes in mice can halt T1D onset [48]. These findings indicate that the connection between the local immune system in the pancreas and the peripheral nervous system plays an important role in the development of autoimmune disease. This connection may involve norepinephrine (NE) signaling, where NE is produced by neurons but locally regulated by nerve-associated macrophages,

potentially through β2 adrenergic signaling, as observed in hypertension [50]. This mechanism may explain how CgA and CST influence autoimmune disease development since 1) NE levels are high in CgA-KO and CST-KO mice, 2) both KO mice are characterized with hypertension and, 3) CgA and CST levels are elevated in autoimmune diseases. Clarification of this link between CgA/CST and autoimmune disease development through catecholamine signaling among nerves, immune cells, and endocrine cells could provide novel insights into therapeutic strategies for autoimmune diseases in the future.

Altogether our findings contribute to better understanding of CgA and CST on the complex neuro-immune-endocrine pancreatic environment. This knowledge is important to develop new treatments to both detect and possibly prevent diseases with a complex neuro-immune-endocrine interplay. In the future, this will hopefully result in the development of better treatment of patients with autoimmune diseases.

4 Material and Methods

4.1 Mice

Male wild type (WT), CgA- knockout (KO) mice and CST-KO mice (3 months old) on C57BL/6 background were kept in a 12 hours dark/light cycle on normal chow diet (NCD: 13.5% calorie from fat; LabDiet 5001, Lab Supply, Fort Worth, TX). These mouse studies were approved by the UCSD and Veteran Affairs San Diego Institutional Animal Care and Use Committees and conform to relevant National Institutes of Health guidelines. Organs were harvested after deeply anesthetizing the mice with isoflurane followed by cervical dislocation. For the immunoblotting experiments organs (adrenal gland, pancreas, bone marrow) were harvested from Male C57BL/6J mice (Taconic, Denmark). These studies were approved by the Regional Animal Ethics committee in Uppsala, Sweden (ethic permit No: 5.8.18-01462/2023)

4.2 Tissue preparation for immunohistochemistry

Pancreata where harvested from WT, CST -KO, and CgA-KO mice. Pancreata were cut in two parts and snap frozen. For immunostainings, the pancreata were imbedded in O.C.T, sectioned in 10 µm sections at -20°C and captured on microscope glass slides (Epredia; J1830AMNZ). For mass spectrometry imaging, the frozen pancreas tissues were sectioned at a thickness of 12 µm using a Leica CM3050S cryostat set at -20°C, and subsequently stored at -80°C until further analysis.

4.3 Fluorescent staining of the pancreatic islets.

Pancreatic sections were fixed for 10 min in 4% paraformaldehyde (PFA) followed by washes in phosphate-buffered saline with 0.1% Tween (PBST) (Medicago; 274713; SIGMA-ALDRICH; SZBA3190V). Afterwards slides where treated for 10 min with 0.2% Triton X100, followed by 30 min in blocking solution (PBS supplemented with FBS 2%, saponin 0.2%, NaAz 0.1%, 1:1000 FC blocker (BD Bioscience; 553142)). To prevent antibody cross-reactivity, the insulin staining was performed first. To do so, slides were incubated o.n. (overnight) at 4˚C with guinea pig insulin primary antibody in blocking buffer (1:1000, Fitzgerald; 20-IP35). The next day, slides were washed three times with PBST for 5 min followed by staining for 30 min at r.t. with the secondary antibody anti-guinea pig-488 (1:500, Invitrogen; A-11073). After washing three times, slides were incubated for 1 hour at r.t. with either mouse anti-glucagon 1:200 (1:200, Proteintech; 67286-1-Ig) and rabbit anti-somatostatin (1:500, Abcam; ab111912) or rabbit anti-

336 norephrine transporter (1:200, Abcam; ab254361) and rat anti-IBA1 (1:1000, Synaptic
337 Systems; 234017) or rabbit anti-Tyrosine Hydroxylase (Abcam; ab137869). Slides were
338 washed three times with PBST for 5 min followed by staining for 30 min at r.t. with anti-
339 mouse 555 (1:1000, Invitrogen; A21127) and anti-rabbit-647 (1:2000, Invitrogen; A31573)
340 or anti-rabbit 555 (1:1000, Invitrogen; A31572) and anti-rat-647 (1:1000, Invitrogen;
341 A48272). After washing three times with PBST, the slides were stained for 10 min with
342 Hoechst (1:10.000, ThermoFisher; 33342) to visualize the nuclei. Afterwards, slides were
343 washed three times with PBS. After the final wash the cover glass (24x50 mm, VWR; 631-
344 0147) was applied using ProLong™ Gold Antifade Mountant (ThermoFisher; P36934). For
345 imaging, the slide scanner Zeiss Axio Scan Z1 with a 20x objective was used.
346
347 **4.4 Analysis of insulin, glucagon and somatostatin cells in the pancreatic islet.**
348 Slide scanner pictures were analysed using Qupath [51]. Islets were annotated based on
349 staining in all channels visualizing the complete islet. The machine-learning software was
350 trained on WT pancreas images to detect cell number per islet using the Hoechst nuclei
351 staining channel and the following nucleus parameters: background radius: 15 px; median
352 filter radius: 0 px; sigma: 3 px; minimum area: 10 px^2; maximum area: 1,000 px^2;
353 intensity parameters: threshold 100; cell parameters: cell expansion 5 px. The obtained cell
354 classifier was used to determine islet shape features (area, length, circularity, solidity,
355 maximum diameter, minimum diameter, and nucleus/cell area ratio) and to calculate the
356 islet density (islet density= islet area/pancreatic section area). This was followed by
357 obtaining the numbers of insulin, somatostatin, and glucagon-producing cells per islet.
358 Afterwards, insulin, somatostatin and glucagon cell ratios were calculated: Positive cells
359 % per islet = (100/total cell number) *target cell number).
360
361 **4.5 Immunoblotting**
362 Macrophages grown from mouse bone marrow [52] or tissue (medulla, isolated pancreatic
363 islets[53]) were lysed in lysis buffer (1% SDS, 10 mM TrisHCl, pH 6.8). Protein
364 concentration was determined according to manufacturer's instructions (Bio-Rad; 500-
365 0114). Afterwards, for each condition 60µg of protein was loaded and run on 10 % mini-
366 protein TGX gels (Bio-Rad; 4561033) in Tris/Tricine/SDS buffer (Bio-Rad; 1610744)
367 followed by transfer for 60min. at 100V at 4°C in Tris/Glycine buffer (Bio-Rad; 1610771)
368 with methanol (Supelco; 1263283323) using a PVDF membrane. The membranes were
369 taken out the cassette and washed with distilled water, followed by blocking in 3% BSA
370 buffer for one hour at r.t.. Membranes were stained o/n at 4°C with primary antibody rabbit
371 chromogranin A (1:1000, Invitrogen; PA5-35071) or rabbit catestatin (1:1000, Proteintech;
372 289-MM-0288). Next day, the membranes were washed three times quickly and three times
373 for 10 min with TBS-t 0.02%. Followed by staining with secondary goat-a-rabbit antibody
374 1:5000 dilution (IRDye800; P/N 925-32211) for one hour at r.t.. Afterwards, the membrane
375 was again washed 3 times with TBS-t 0.02%. Both membranes were scanned on a Bio-rad
376 ChemiDoc MP imager to visualize the fluorescent staining.
377
378 **4.6 Spatial Mass Spectrometry**
379 Two consequtive 12 µm pancreatic sections were taken containing tissue of 3 WT, 3 CgA-
380 KO and 3 CST-KO mice. One section was stained with hematoxylin-eosin (HE) to identify
381 the pancreatic islets using Qupath. The other slide was used for neurotransmitter analysis
382 of serotonin (5HT), gamma-Aminobutyric acid (GABA), histamine, L-cysteine, taurine,
383 creatine, spermidine, histidine, norepinephrine (NE), L-tyrosine, spermine and
384 hypoxanthine. Derivatization matrix FMP-10 synthesized in house [54] (Sup Table 1) was
385 applied with TM-Sprayer, HTX-Technologies. The spraying method was set up to include

30 passes, with a flow rate of 80 µl/min at a temperature of 80°C. The nozzle velocity was adjusted to 1100 mm/min, while the track spacing was set at 2.0 mm, and N2 was set 6 psi. Full tissue MSI experiments were performed using a timsTOF fleX MS imaging instrument in positive ion mode (Bruker Daltonics GmbH, Bremen, Germany). Online calibration was performed using m/z 555.2231, an abundant ion cluster signal of FMP-10. Data was initially processed with visualization software in flexImaging (v. 5.0., Bruker Daltonics). Islets were mapped on the tissue with 5-HT signal and overlay with stained HE staining. For each islet a corresponding ROI of exocrine tissue was drawn.

4.7 Analysing neurotransmitters in the islets and exocrine pancreas

Islet selections in Qupath were exported using the SciLS^{tm} lab extension (Bruker Daltonics) and imported into the flexImaging (Bruker Daltonics, Bremen, v.5.0) software. To match and optimize the pancreatic islet location from the HE staining, the serotonin signal was used. After identifying the pancreatic islets, annotations were made for the matching exocrine tissue (serotonin negative area). Expression data of neurotransmitters in the pancreatic islet and exocrine tissue was extracted and visualized in graphs.

4.8 Statistical analysis

Data are expressed as mean ± SEM. One-way ANOVA with Bonferroni post-hoc tests or non-parametric Mann-Whitney test were applied for multiple comparisons. A p value of $p < 0.05$ was considered statistically significant.

5 Figure descriptions

Fig. 1 CgA and CST in the pancreatic islet

A) Immunofluorescent staining for catestatin in WT, CgA-KO and CST-KO pancreas **B)** CgA cleavages products towards CST. **C)** Westernblot showing chromogranin A staining in the Medulla, pancreatic islets and macrophages (mac). Arrows indicate full CgA and possible cleavage products of CgA. **D)** Similar membrane stained for catestatin in synthetic catestatin peptide (CST), Medulla, Pancreatic islets and macrophages (mac).

Fig. 2 Composition of pancreatic islets in WT, CgA-KO and CST-KO

A) HE staining of WT, CgA-KO and CST-KO pancreatic slices including annotations for islets (white dotted lines) and blood vessels (B). **B)** Representative pictures of immunofluorescent staining of glucagon (cyan), insulin (green), somatostatin (magenta) and Hoechst (blue) on WT, CgA-KO and CST-KO pancreatic slices. **C)** Islet area **D)** Islet density **E)** Islet circularity **F)** Quantification of alpha/beta/delta/negative cells per islet. Quantification is based on the staining of panel B. N=3 mice per group **G)** Graph displaying glucose tolerance test (GTT) results for WT (black), CgA-KO (pink) and CST-KO (green) over time (min) N=8 per group **H)** Graph displaying area under the curve (mg/dL*min) calculated from the GTT graph of panel G.

Fig. 3 Innervation of pancreatic islets in WT, CgA-KO and CST-KO

A) Representative images of nerve staining (norepinephrine transporter (NET, magenta), islets (insulin, green) and nuclei (Hoechst) in WT, CgA-KO and CST-KO pancreatic slices **B)** Quantification of the nerve ratio in and outside pancreatic islet for WT, CgA-KO and CST-KO based on the staining of panel A. **C)** Quantification of nerve volume in the islet and the exocrine pancreas for WT, CgA-KO and CST-KO. **D)** Representative images of nerve staining (norepinephrine transporter (NET, cyan), macrophages (IBA1, magenta),

islets (insulin, green) and nuclei (gray) in WT, CgA-KO and CST-KO pancreatic slices. **E)** Macrophage count per islet (every dot in the graph represents one islet). **F)** Number of macrophages interacting with nerves per islet for WT, CgA-KO and CST-KO. N=3 mice per group

Fig. 4 Pancreatic neurotransmitter regulation upon CgA or CST knockout.
A) Comparative analysis of analyte regulation in pancreatic tissue models. This figure highlights the log2 fold expression of the analytes in pancreatic tissue of WT (gray), CgA-KO (pink) and CST-KO (blue). **B)** Comparative analysis of analyte Regulation in pancreatic tissue models. This figure highlights the differential expression of neurotransmitters between pancreatic islets (blue) and adjacent exocrine tissue (red), based on the average intensity of RMS normalized regions.

Fig. 5 Islet and exocrine pancreatic neurotransmitter regulation upon CgA or CST knockout.
A) Serotonin heatmap showing examples of WT (green), CgA-KO (red) and CST-KO (yellow) pancreatic slices including annotations for islets (colored) or exocrine tissue (white). **B)** Peak area for islets and exocrine tissue of WT, CgA-KO and CST-KO pancreas of serotonin, **C)** Taurine **D)** GABA **E)** Histamine **F)** Cysteine **G**) Spermidine and spermine. Spermidine can be converted into spermine as illustrated in the schematic drawing. N= 3 mice per group

Fig. 6 Islet and exocrine pancreatic neurotransmitter regulation upon CgA or CST knockout.
A) Peak area of norepinephrine for islets and exocrine tissue of WT, CgA-KO and CST-KO pancreas **B)** Creatine **C)** Hypoxantine. N= 3 mice per group $P<0.05$ = *

6 Figures

Fig. 1

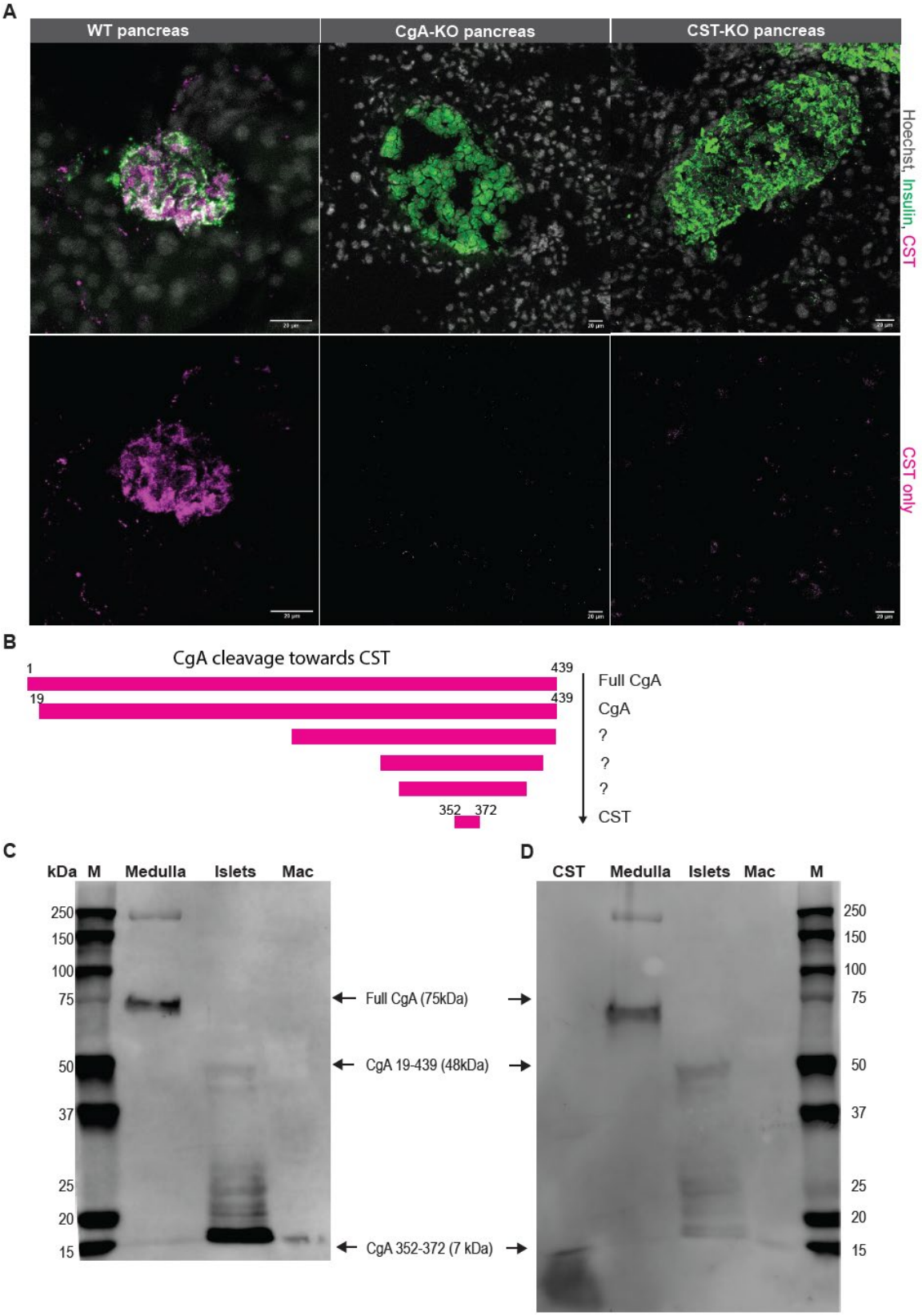
A
WT pancreas
CgA-KO pancreas
CST-KO pancreas
Hoechst, Insulin, CST
CST only
B
CgA cleavage towards CST
1
439
19
439
352
372
Full CgA
CgA
?
?
?
CST
C
kDa
M
Medulla
Islets
Mac
250
150
100
75
50
37
25
20
15
Full CgA (75kDa)
CgA 19-439 (48kDa)
CgA 352-372 (7 kDa)
D
CST
Medulla
Islets
Mac
M
250
150
100
75
50
37
25
20
15

Fig. 2

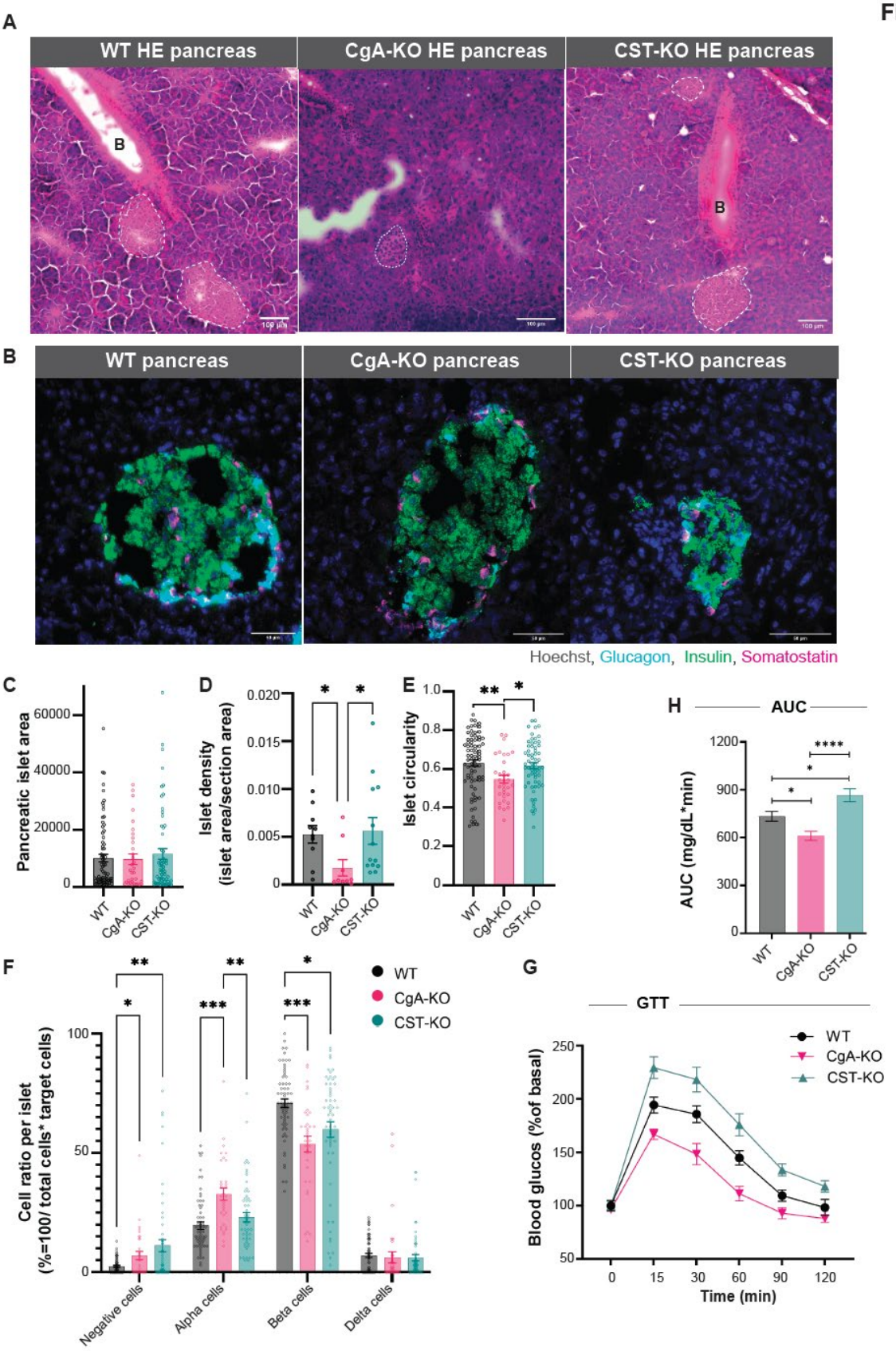
A
WT HE pancreas
CgA-KO HE pancreas
CST-KO HE pancreas
B
B
WT pancreas
CgA-KO pancreas
CST-KO pancreas
Hoechst, Glucagon, Insulin, Somatostatin
C
Pancreatic islet area
60000
40000
20000
0
WT
CgA-KO
CST-KO
D
Islet density
(islet area/section area)
0.020
0.015
0.010
0.005
0
*
*
WT
CgA-KO
CST-KO
E
Islet circularity
1.0
0.8
0.6
0.4
0.2
0
**
*
WT
CgA-KO
CST-KO
H
AUC
AUC (mg/dL*min)
1200
900
600
300
0
****
*
*
WT
CgA-KO
CST-KO
F
Cell ratio per islet
(%=100/ total cells* target cells)
100
50
0
*
**
***
**
***
*
WT
CgA-KO
CST-KO
Negative cells
Alpha cells
Beta cells
Delta cells
G
GTT
Blood glucos (%of basal)
250
200
150
100
50
WT
CgA-KO
CST-KO
0
15
30
60
90
120
Time (min)

Fig. 3

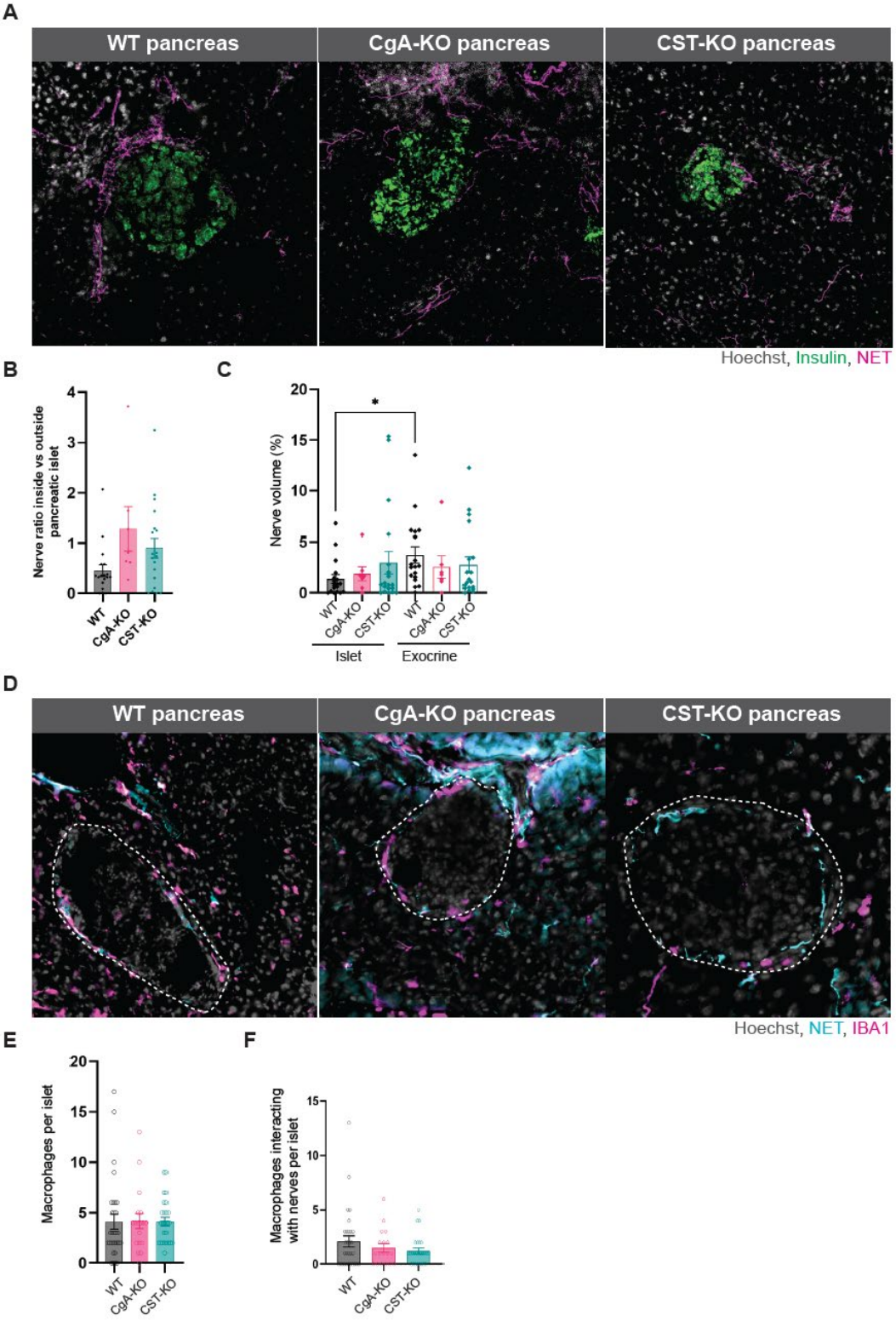
A
WT pancreas
CgA-KO pancreas
CST-KO pancreas
Hoechst, Insulin, NET
B
Nerve ratio inside vs outside pancreatic islet
WT
CgA-KO
CST-KO
C
Nerve volume (%)
*
Islet
Exocrine
D
WT pancreas
CgA-KO pancreas
CST-KO pancreas
Hoechst, NET, IBA1
E
Macrophages per islet
F
Macrophages interacting with nerves per islet

Fig. 4

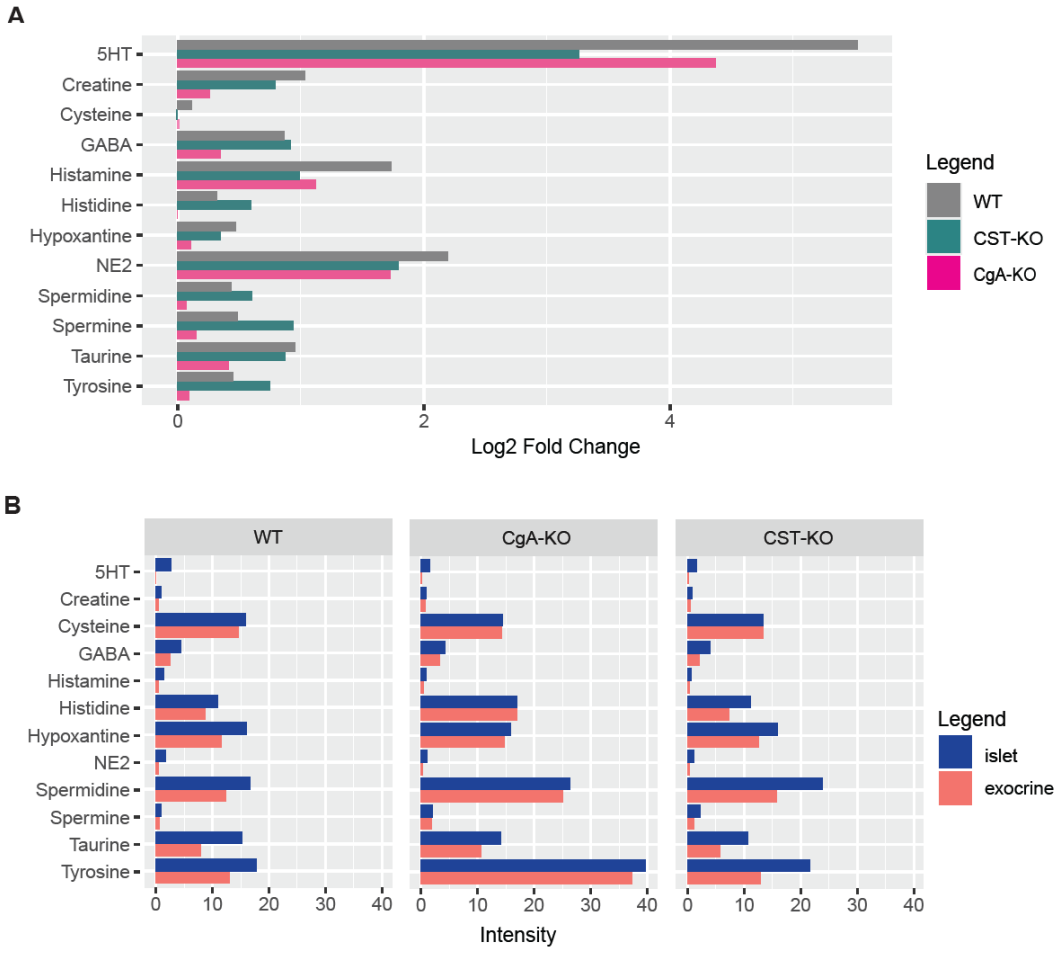
A
5HT
Creatine
Cysteine
GABA
Histamine
Histidine
Hypoxantine
NE2
Spermidine
Spermine
Taurine
Tyrosine
0
2
4
Log2 Fold Change
Legend
WT
CST-KO
CgA-KO
B
WT
CgA-KO
CST-KO
5HT
Creatine
Cysteine
GABA
Histamine
Histidine
Hypoxantine
NE2
Spermidine
Spermine
Taurine
Tyrosine
0
10
20
30
40
Intensity
Legend
islet
exocrine

Fig. 5

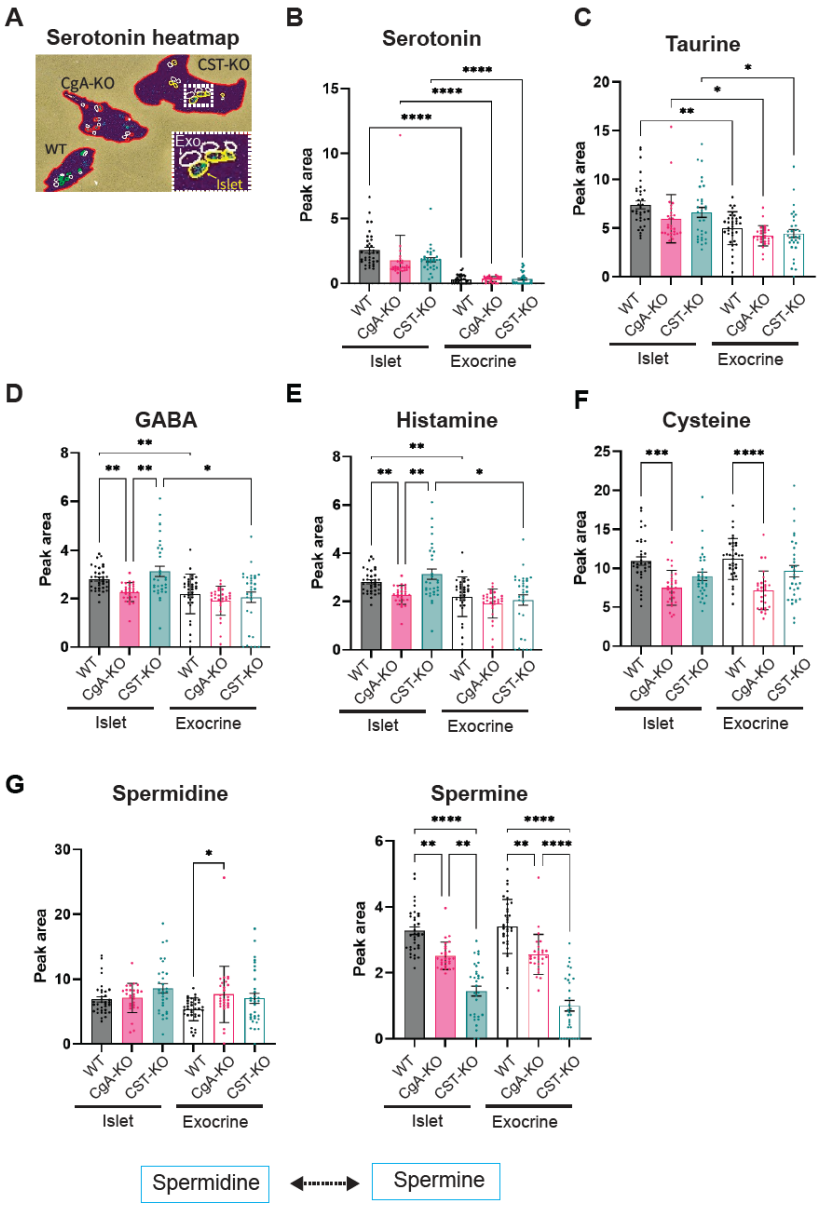
A
Serotonin heatmap
CST-KO
CgA-KO
WT
Exo
Islet
B
Serotonin
Peak area
C
Taurine
D
GABA
E
Histamine
F
Cysteine
G
Spermidine
Spermine
WT
CgA-KO
CST-KO
Islet
Exocrine
Spermidine
Spermine

Fig. 6

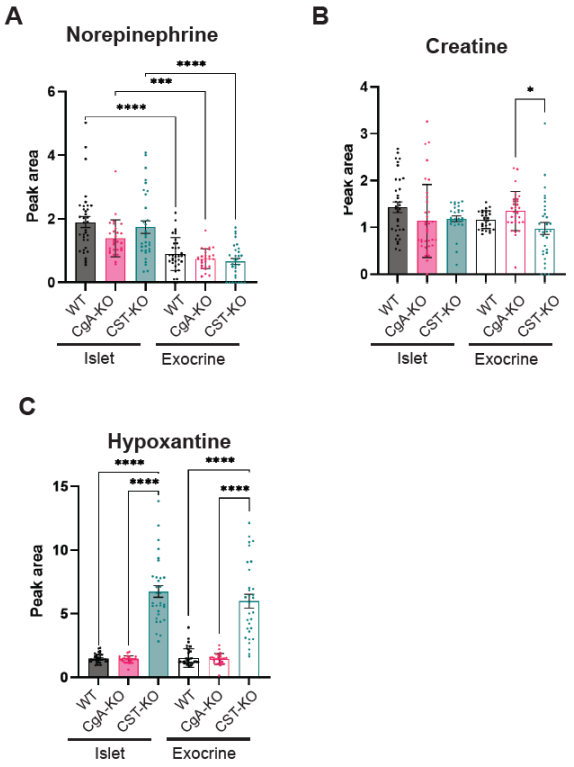

468
469
470 # 7 Conflict of Interest
471 SKM is the founder of CgA Therapeuticals, Inc. and co-founder of Siraj Therapeutics, Inc. The
472 authors declare that the research was conducted in the absence of any commercial or financial
473 relationships that could be construed as a potential conflict of interest.
474
475 # 8 Author Contributions
476 S.K.M. has taken care of the mice and harvested the pancreata. E.M.M, D.E and M.B. have
477 performed the HE stainings, fluorescent staining's and islet quantifications. D.E. has performed
478 the immunoblotting. M.N. and A.N. sectioned, prepared and run the pancreatic slices in the
479 Maldi-MS. M.N., A.F. and E.J. performed data analysis. E.M.M. assisted with data
480 interpretation and compiled the manuscript. G.C., S.M.K and E.J. provided expertise. All
481 authors contributed in writing and editing the manuscript.
482
483 # 9 Funding
484 E.M. is funded by a Rubicon grant from the Netherlands Organization for Scientific Research
485 (NWO) and the Swedish Research Council. G.C. is supported by grants from the Swedish
486 Research Council, the Swedish Society for Medical Research and the Göran Gustafsson
487 foundation. SKM is supported by grants from the National Institutes of Health (1 R21
488 AG072487-01, 1 R21 AG080246-01, 1 R21 AG078635-01A1). This study was supported by
489 Science for Life Laboratory (SciLifeLab) and Uppsala University Research Infrastructure
490 funding.
491
492

10 References

1. Rorstad, O. (2005) Prognostic indicators for carcinoid neuroendocrine tumors of the gastrointestinal tract. *J. Surg. Oncol.* 89, 151–160
2. O'Connor, D.T. (1985) Plasma chromogranin A. Initial studies in human hypertension. *Hypertension* 7, I76-9
3. Zuetenhorst, J.M. *et al.* (2004) Role of natriuretic peptides in the diagnosis and treatment of patients with carcinoid heart disease. *Br. J. Cancer* 90, 2073–2079
4. Ceconi, C. (2002) Chromogranin A in heart failure. A novel neurohumoral factor and a predictor for mortality. *Eur. Heart J.* 23, 967–974
5. O'Connor, D.T. *et al.* (1989) Rapid radioimmunoassay of circulating chromogranin A: In vitro stability, exploration of the neuroendocrine character of neoplasia, and assessment of the effects of organ failure. *Clin. Chem.* 35, 1631–1637
6. Muntjewerff, E.M. *et al.* (2021) Chromogranin A regulates gut permeability via the antagonistic actions of its proteolytic peptides. *Acta Physiol.* 232
7. Di Comite, G. *et al.* (2009) Circulating chromogranin A reveals extra-articular involvement in patients with rheumatoid arthritis and curbs TNF-α-elicited endothelial activation. *J. Leukoc. Biol.* 85, 81–87
8. Hsu, C.-H. *et al.* (2015) Chromogranin A levels and mortality in patients with severe sepsis. *Biomarkers* 20, 171–176
9. Bousiges, O. *et al.* (2024) Diagnostic value of CSF chromogranin A to discriminate between Alzheimer's disease and dementia with Lewy bodies. *Neuropathol. Appl. Neurobiol.* 50, 1–157
10. Muntjewerff, E.M. *et al.* (2022) Putative regulation of macrophage-mediated inflammation by catestatin. *Trends Immunol.* 43, 41–50
11. Kojima, M. *et al.* (2018) Catestatin Prevents Macrophage-Driven Atherosclerosis but Not Arterial Injury–Induced Neointimal Hyperplasia. *Thromb. Haemost.* 118, 182–194
12. Ying, W. *et al.* (2018) Catestatin Inhibits Obesity-Induced Macrophage Infiltration and Inflammation in the Liver and Suppresses Hepatic Glucose Production, Leading to Improved Insulin Sensitivity. *Diabetes* 67, 841–848
13. Ying, W. *et al.* (2021) Immunosuppression of Macrophages Underlies the Cardioprotective Effects of CST (Catestatin). *Hypertension* 77, 1670–1682
14. Mahata, S.K. *et al.* (2018) Catestatin: A Master Regulator of Cardiovascular Functions. *Curr. Med. Chem.* 25, 1352–1374
15. Ying, W. *et al.* (2018) Catestatin Inhibits Obesity-Induced Macrophage Infiltration and Inflammation in the Liver and Suppresses Hepatic Glucose Production, Leading to Improved Insulin Sensitivity. *Diabetes* 67, 841–848
16. Simac, P. *et al.* (2022) Serum catestatin levels in patients with rheumatoid arthritis. *Sci. Rep.* 12, 3812–3812
17. Schneider, F. *et al.* (2022) Assessment of plasma Catestatin in COVID-19 reveals a hitherto unknown inflammatory activity with impact on morbidity-mortality. *Front. Immunol.* 13, 985472–985472
18. Borovac, J.A. *et al.* (2019) Catestatin in Acutely Decompensated Heart Failure Patients: Insights from the CATSTAT-HF Study. *J. Clin. Med.* 8, 1132
19. Xu, W. *et al.* (2016) Plasma Catestatin: A Useful Biomarker for Coronary Collateral Development with Chronic Myocardial Ischemia. *PLoS One* 11, e0149062
20. Meng, L. *et al.* (2011) Plasma catecholamine release-inhibitory peptide catestatin in patients with essential hypertension. *J. Cardiovasc. Med.* 12, 643–647
21. Liu, L. *et al.* (2013) Plasma levels and potential roles of catestatin in patients with

coronary heart disease. *Scand. Cardiovasc. J.* 47, 217–224
22. Zhu, D. *et al.* (2015) Correlation of Plasma Catestatin Level and the Prognosis of Patients with Acute Myocardial Infarction. *PLoS One* 10, e0122993
23. O'connor, D.T. *et al.* (2008) Heritability and Genome-Wide Linkage in US and Australian Twins Identify Novel Genomic Regions Controlling Chromogranin A Implications for Secretion and Blood Pressure. DOI: 10.1161/CIRCULATIONAHA.107.709105
24. Fung, M.M. *et al.* (2010) Direct Vasoactive Effects of the Chromogranin A (CHGA) Peptide Catestatin in Humans In Vivo. *Clin. Exp. Hypertens.* 32, 278–287
25. Mahapatra, N.R. *et al.* (2005) Hypertension from targeted ablation of chromogranin A can be rescued by the human ortholog. *J. Clin. Invest.* 115, 1942–1952
26. Gayen, J.R. *et al.* (2010) Role of Reactive Oxygen Species in Hyperadrenergic Hypertension. *Circ. Cardiovasc. Genet.* 3, 414–425
27. Avolio, E. *et al.* (2014) Antihypertensive and neuroprotective effects of catestatin in spontaneously hypertensive rats: interaction with GABAergic transmission in amygdala and brainstem. *Neuroscience* 270, 48–57
28. Rabbi, M.F. *et al.* (2017) Reactivation of Intestinal Inflammation Is Suppressed by Catestatin in a Murine Model of Colitis via M1 Macrophages and Not the Gut Microbiota. *Front. Immunol.* 8
29. Rabbi, M.F. *et al.* (2014) Catestatin decreases macrophage function in two mouse models of experimental colitis. *Biochem. Pharmacol.* 89, 386–398
30. Portela-Gomes, G.M. *et al.* (2008) The importance of chromogranin A in the development and function of endocrine pancreas. *Regul. Pept.* 151, 19–25
31. Brereton, M.F. *et al.* (2014) Reversible changes in pancreatic islet structure and function produced by elevated blood glucose. *Nat. Commun. 2014 51* 5, 1–11
32. Nakagawa, R. *et al.* (2023) Circularity of islets is a distinct marker for the pathological diagnosis of adult non-neoplastic hyperinsulinemic hypoglycemia using surgical specimens. *Diagn. Pathol.* 18
33. Gayen, J.R. *et al.* (2009) A Novel Pathway of Insulin Sensitivity in Chromogranin A Null Mice. *J. Biol. Chem.* 284, 28498–28509
34. Hampton, R.F. *et al.* (2022) Unravelling innervation of pancreatic islets. *Diabetologia* 65, 1069
35. Bak, D.W. *et al.* (2019) Cysteine Reactivity Across the Sub-Cellular Universe. *Curr. Opin. Chem. Biol.* 48, 96
36. Marselli, L. *et al.* (2021) Arginase 2 and polyamines in human pancreatic beta cells: Possible role in the pathogenesis of type 2 diabetes. *Int. J. Mol. Sci.* 22, 12099
37. Sharp, G.W.G. and Straub, S.G. (2012) Evolving insights regarding mechanisms for the inhibition of insulin release by norepinephrine and heterotrimeric G proteins. *Am. J. Physiol. - Cell Physiol.* 302, 1687–1698
38. Abramov, G. *et al.* (2022) Intermediate products of purine metabolism in an experimental model of pancreatic necrosis. *Acta Bio Medica Atenei Parm.* 93, 2022298
39. Wollam, J. *et al.* (2017) Chromogranin A regulates vesicle storage and mitochondrial dynamics to influence insulin secretion. *Cell Tissue Res.* 368, 487–501
40. Hougaard, D.M. and Larsson, L.I. (1986) Localization and possible function of polyamines in protein and peptide secreting cells. *Med. Biol.* 64, 89–94
41. Hougaard, D.M. *et al.* (1986) Localization and biosynthesis of polyamines in insulin-producing cells. *Biochem. J.* 238, 43—47
42. Sjöholm, A. (1993) Role of polyamines in the regulation of proliferation and hormone production by insulin-secreting cells. *Am. J. Physiol.* 264, C501-18

43. Welsh, N. and Sjöholm, A. (1988) Polyamines and insulin production in isolated mouse pancreatic islets. *Biochem. J.* 252, 701—707
44. Welsh, N. (1990) A role for polyamines in glucose-stimulated insulin-gene expression. *Biochem. J.* 271, 393–397
45. Sjöholm, Å. *et al.* (2001) Polyamines in pancreatic islets of obese-hyperglycemic (ob/ob) mice of different ages. *Am. J. Physiol. - Cell Physiol.* 280
46. Lenzen, S. and Rustenbeck, I. (1991) Effects of IP3, Spermine, and Mg2+ on Regulation of Ca2+ Transport by Endoplasmic Reticulum and Mitochondria in Permeabilized Pancreatic Islets. *Diabetes* 40, 323–326
47. Guyot, M. *et al.* (2019) Pancreatic nerve electrostimulation inhibits recent-onset autoimmune diabetes. *Nat. Biotechnol.* 37, 1446–1451
48. Christoffersson, G. *et al.* (2020) Interference with pancreatic sympathetic signaling halts the onset of diabetes in mice. *Sci. Adv.* 6
49. Taborsky, G.J. *et al.* (2014) The p75 neurotrophin receptor is required for the major loss of sympathetic nerves from islets under autoimmune attack. *Diabetes* 63, 2369–2379
50. Grisanti, L.A. *et al.* (2016) Leukocyte-Expressed β2-Adrenergic Receptors Are Essential for Survival after Acute Myocardial Injury. *Circulation* 134, 153–167
51. Bankhead, P. *et al.* (2017) QuPath: Open source software for digital pathology image analysis. *Sci. Reports 2017 71* 7, 1–7
52. Haag, S.M. and Murthy, A. (2021) Murine monocyte and macrophage culture. *Bio-protocol* 11
53. Bohman, S. *et al.* (2006) No differences in efficacy between noncultured and cultured islets in reducing hyperglycemia in a nonvascularized islet graft model. *Diabetes Technol. Ther.* 8, 536–545
54. Shariatgorji, M. *et al.* (2019) Comprehensive mapping of neurotransmitter networks by MALDI–MS imaging. *Nat. Methods 2019 1610* 16, 1021–1028